

Hydrodynamic Interactions in Protein Folding

Marek Cieplak and Szymon Niewieczerzał

*Institute of Physics,
Polish Academy of Sciences,
Al. Lotników 32/46,
02-668 Warsaw, Poland*

Abstract

We incorporate hydrodynamic interactions (HI) in a coarse-grained and structure-based model of proteins by employing the Rotne-Prager hydrodynamic tensor. We study several small proteins and demonstrate that HI facilitate folding. We also study HIV-1 protease and show that HI make the flap closing dynamics faster. The HI are found to affect time correlation functions in the vicinity of the native state even though they have no impact on same time characteristics of the structure fluctuations around the native state.

I. INTRODUCTION

Globular proteins acquire distinct compact native conformations in water as a result of the hydrophobic effect. Another role of water is to mediate the hydrodynamic interactions (HI) between moving amino acids in analogy to the HI in polymers^{1,2} and between particles in colloidal suspensions^{3,4,5,6,7,8}. One expects that the HI should generally enhance cooperative features in the dynamics of proteins, but it is not clear in what way, exactly, will this show. In the case of mechanically-induced unfolding, the HI have been found to lead to a) reduction in peak unfolding forces when stretching at high steady velocities⁹, b) reduction in unfolding times when stretching at constant force⁹ because of the dragging effect, and c) hindering of unravelling imposed through uniform¹⁰ and shear¹¹ fluid flows because of the screening effects.

In this paper, we focus on the kinetics of folding and of fluctuational motions around the native state. We assess the relevance of HI in these phenomena within the previously used coarse-grained implicit-solvent model of proteins^{12,13,14,15} of N beads with the Lennard-Jones contact interactions. As in refs.^{9,10}, the HI are introduced through the Rotne-Prager tensor^{16,17}.

Kikuchi et al.¹⁸ have taken another approach to introduce the fluid-related effects. Instead of employing the tensorial field they make use of the stochastic rotation dynamics²². They have demonstrated that HI facilitate the collapse transition of a self-attracting homopolymer because of dragging effect in which a bead attracted to another bead through, say, the Lennard-Jones potential drags the fluid containing other beads with it. They have also, together with a related thesis work of Ryder¹⁹, reported a small, of order 10%, reduction in the folding time, t_{fold} , in simple models of several proteins, such as 2ci2. On the other hand, Baumketner and Hiwatari²⁰ claim otherwise, pointing out that HI give rise to the effective repulsion between two beads which are coming towards each other, thus slowing down the collapse. They consider a simplified "minimal" model introduced in ref.²¹. For a short β -hairpin, they obtain a certain increase in the folding time and lack of any effect for a short α -helix.

Here, we consider four short proteins, 1l2y ($N=20$), 1bba ($N=36$), 1crn ($N=46$) 2ci2 ($N=65$) and one β -hairpin ($N=14$) – a fragment of the 1gb1 protein. In each case, our results are consistent with the picture of Kikuchi et al.¹⁸. The collapse phase of the folding

process is indeed faster. However, we find the reduction in t_{fold} to be more substantial than in the work of Ryder¹⁹, for instance, by a factor, f , of 2 for 1crn. Possible reasons for this quantitative discrepancy include differences in the shape of the initial conformations (Ryder may have more compact starting conformations compared to the fully extended situations considered here) and in the precise nature of the folding criterion (Ryder may have a criterion based on a characteristic size of a distance deviation from the native state as opposed to the contact-based criterion we use). Our results differ qualitatively with that of ref.²⁰. It should be noted that the model used there comes with attractive contacts only between hydrophobic amino acids and requires this attraction to be the strongest at the distance of 4.2 Å between the corresponding C $^{\alpha}$'s. In proteins, contact distances between the C $^{\alpha}$ atoms extend in fact from 4.4 to 12.8 Å²³ which is likely to change the nature of the effects associated with the HI. In fact, when we a) constrain the potentials for the *beta*-hairpin case to have a minimum at 4.2 Å the reduction factor goes down to 1.2 and then, in addition, b) increase the number of allowed contacts to imitate the situation envisioned within the minimal model, f becomes equal to 0.87, indicating that the HI make the folding longer. Thus the result of ref.²⁰ is related to the minimal nature of the model considered there.

We then consider a larger protein – the HIV-1 protease (1a30). This protein is a homodimer and each of the two chains comprises 98 amino acids. Its active site is covered by two flexible β -hairpins, called flaps, that control the entry of a polypeptide substrate. The flap opening dynamics in this protein has been studied before within all atom²⁴ and coarse-grained molecular dynamics schemes. Here, we pull the flaps apart and then monitor their return to the native form as a function of time. We observe that the HI make the flap closing faster.

Finally, we return to the small protein 1l2y and investigate fluctuations around the native state by considering single- and double-residue characteristics of these fluctuations. We find that the HI have no impact on their same-time averages. This result is not surprising because, in the overdamped limit considered here, the equilibrium distributions of conformations are the same. However, it sets the stage for the observation that time correlation functions are sensitive to the HI despite the protein being essentially folded.

II. METHODS

The coarse-grained, Go-type model²⁸ of a protein we use is constructed based on the knowledge of the native state. There are many ways to implement it. Examples are given in refs.^{21,29,30,31,32,33}. The details of the particular implementation we use are described in^{14,33}. Each residue is represented by a single bead centered on the position of the C α atom. The successive beads along the backbone are tethered by harmonic potentials with a minimum at 3.8 Å and they are also endowed with the chirality based local backbone stiffness¹⁴. The other interactions between the residues i and j are split into two classes: native and non-native as described in ref.¹⁴. The native contacts are endowed with the effective Lennard-Jones potential $V_{ij} = 4\epsilon \left[\left(\frac{\sigma_{ij}}{r_{ij}} \right)^{12} - \left(\frac{\sigma_{ij}}{r_{ij}} \right)^6 \right]$ whereas the non-native contacts are purely repulsive. The length parameters σ_{ij} are chosen so that the potential minima correspond, pair-by-pair, to the experimentally established native distances between the respective aminoacids. The energy parameter, ϵ , is taken to be uniform and $0.3\epsilon/k_B$ is usually playing the role of the room temperature¹⁵.

The time evolution is described by the Brownian dynamics (BD)³⁴. The displacement of particle i in time step Δt obeys

$$\mathbf{r}_i - \mathbf{r}_i^0 = \sum_j (\nabla_j \cdot \mathbf{D}_{ij}^0) \Delta t + \frac{1}{k_B T} \sum_j \mathbf{D}_{ij}^o \cdot \mathbf{F}_j^0 \Delta t + \mathbf{B}_i, \quad (1)$$

where the index 0 denotes the values of respective quantities at the beginning of the time step, \mathbf{F}_j is the force exerted on particle j by other particles, and T is temperature. \mathbf{D} is a diffusion tensor and \mathbf{B} - a random displacement given by a Gaussian distribution with an average value of zero and covariance obeying

$$\langle \mathbf{B}_i \mathbf{B}_j \rangle = 2\mathbf{D}_{ij}^0 \Delta t. \quad (2)$$

If the diffusion tensor is nondiagonal, there exists a hydrodynamic coupling between particles i and j (*cf.* Eq.1). We take the diffusion tensor in the form^{16,17}

$$\mathbf{D}_{ii} = \frac{k_B T}{\gamma} \mathbf{I} \quad (3)$$

and

$$\mathbf{D}_{ij} = \frac{k_B T}{\gamma} \frac{3a}{4r_{ij}} \begin{cases} \left[\left(1 + \frac{2a^2}{3r_{ij}^2} \right) \mathbf{I} + \left(1 - \frac{2a^2}{r_{ij}^2} \right) \hat{\mathbf{r}}_{ij} \hat{\mathbf{r}}_{ij} \right], & r_{ij} \geq 2a \\ \frac{r_{ij}}{2a} \left[\left(\frac{8}{3} - \frac{3r_{ij}}{4a} \right) \mathbf{I} + \frac{r_{ij}}{4a} \hat{\mathbf{r}}_{ij} \hat{\mathbf{r}}_{ij} \right], & r_{ij} < 2a \end{cases} \quad (4)$$

where $\mathbf{r}_{ij} = \mathbf{r}_j - \mathbf{r}_i$, a is the hydrodynamic radius, and γ is the damping constant. By Stokes's law, $\gamma = 6\pi a\eta$, where η is the viscosity of the fluid. The characteristic time scale in the problem, τ , is of order 1 ns, which reflects duration of a diffusional passage of a typical contact distance ($\sim 5 \text{ \AA}$).

The situation corresponding to the lack of HI will be denoted by BD (for Brownian dynamics) and will be implemented by setting \mathbf{D}_{ij} ($i \neq j$) to zero. The selection of the value of the hydrodynamic radius is not obvious and more studies are needed to settle this issue. We just want to determine qualitatively what would happen if it was non-zero. When one thinks of amino acids as represented by spheres then one would expect that a should not exceed a half of the distance between consecutive C^α 's. Thus we consider the hydrodynamic radius of 1.5 \AA to have a substantial enough and yet satisfying this criterion. On the other hand, the side groups extend laterally and may produce a correspondingly larger drag force. It has been argued^{35,36} that a characteristic a of an amino acid could be even as big as 4.2 \AA whereas a characteristic van der Waals radius is about 3.0 \AA ³⁷. The van der Waals volume does not include hydration layers. Such big values would mean existence of an overlap between spheres in a chain, but its usage takes into account the non-spherical properties of the amino acids in an approximate way. Considering a of 1.5 \AA has a numerical advantage because the time unit is governed by the damping constant and is thus proportional to a . Thus the folding times are expected to scale linearly with a for systems both with and without HI, making it relevant to assess the role of HI regardless the particular choice of a . It cannot be ruled out, however, that HI may introduce some corrections to scaling. Assessment of such corrections would need a separate study.

It should be noted that there are some amino acid to amino acid variations in the values of the van der Waals and the de la Torre - Bloomfield³⁵ hydrodynamic radii. For glycine, alanine, and arginine, the former are 2.4 \AA , 2.6 \AA , and 3.3 \AA respectively, and the latter are 3.6 \AA , 3.7 \AA , and 4.5 \AA respectively³⁸. These variations are not expected to affect the findings in analogy to the lack of sensitivity to the variations in the values of the masses¹³ or in the values of the damping constant³⁹. A scaling by the mean value of the parameters has been demonstrated in these other cases.

Throughout this paper we employ the Brownian dynamics evolution algorithm since it allows for a straightforward incorporation of the HI. However, all of the BD results obtained here are reproduced by the Langevin dynamics algorithm as used in refs.^{13,14}. The Langevin

dynamics involves inertia but the system is overdamped.

III. RESULTS

A. Kinetics of folding

Figure 1 shows the T -dependence of the median value of t_{fold} determined as the first time to establish all native contacts ($r_{ij} < 1.5\sigma_{ij}$). For each of the proteins studied, there is a broad plateau of optimal folding. In the optimal regime, t_{fold} with HI is shorter by a factor f than in the BD case. The value of the factor depends on the protein and is indicated on the right hand side of the figure. For the β -hairpin, f is 1.3. The largest protein studied, 2ci2, has been simulated only at one temperature ($0.3 \epsilon/k_B$). The simulations yielded t_{fold} of $\sim 840\tau$ and $\sim 470\tau$ for the BD and HI models respectively. The corresponding f factor of 1.8 is clearly distinct from ~ 1.1 found in ref.¹⁹. The discrepancy may probably be attributed to two circumstances: a) the statistics involved in ref.¹⁹ have been restricted to several trajectories, b) the values of f depend on the nature of the starting conformations. The bigger the number of the native contacts that are present in the initial stages of folding, the smaller the value of f . In our simulations, the starting conformations are fully extended.

The HI-induced acceleration of folding is governed mostly by the initial collapse as illustrated for two typical trajectories for 1crn in the bottom panel of Figure 2. This figure shows the time evolution of the radius of gyration, R_g . Qualitatively, the collapsed phase is said to be reached when R_g does not exceed 15% of its native value. In agreement with ref.¹⁸, the HI are seen to significantly accelerate arrival at the collapsed phase (by a factor larger, ~ 2.6 , than the acceleration factor found for t_{fold}). The subsequent establishment of contacts involves a stochastic search in the conformational space and is not affected by any hydrodynamic effects.

The top panel of Figure 2 shows the distributions of the values of t_{fold} across 100 trajectories for 1crn. The distributions are non-Gaussian and have pronounced tails. The peak of the distribution corresponding to HI is at shorter times than BD, but the long-time ends are comparable. It should be noted that both at high and low temperature ends, when the folding time becomes large, the distinction between the HI and BD cases evaporates because when the protein kinetics are slow the related induced fluid flows are sluggish.

Figure 3 shows the scenario diagram¹⁴ which represents the first times needed to establish specific native contacts as averaged over the trajectories. The native contacts are labelled by their sequential separation $|j-i|$. It is seen that the presence of HI accelerates establishment of all contacts without changing the order in which they are set. The same statement applies to the other proteins we have studied and we expect it to hold in general.

B. Closing of flaps in HIV-1 protease

The native structure of HIV-1 protease is schematically represented by the lower right conformation shown in Figure 4. The hairpin fragments that form the flaps are highlighted by showing the corresponding C $^{\alpha}$ atoms. The locations of the flaps can be conveniently described by providing coordinates of the four-atom centers of mass. The two centers of mass are $R_{f,nat}=4.09 \text{ \AA}$ away from each other. We pull the model flaps apart by exerting a stretching force applied along the direction that links the initial centers of mass of the two flaps until they are separated by 32.75 \AA . The resulting conformation is shown on the upper left in Figure 4. The force is then removed and we monitor the distance, R_f , between the centers of mass as a function of time.

Figure 4 demonstrates that the HI make the closing of the flaps faster. The value of $R_f = 2R_{f,nat}$ is reached about twice as fast with HI compared to the BD case. The phenomenon is analogous to refolding discussed previously. However, it affects only a part of the full protein.

C. Structure fluctuations around the native state

We now consider 1l2y which is the smallest among the set of proteins studied here so that an appropriate conformational statistics can be generated. Its native structure is shown in Figure 5. It is akin to a β -hairpin in which one of the "arms", however, is shaped into an α -helix. The 20 amino acids are enumerated from the helical end. We set the protein in its native conformation, then evolve it at $T=0.3\epsilon/k_B$ in four different trajectories which last for $200\,000 \tau$.

1. Equal time characteristics

One way to quantify the dynamics of the motion around the native state is to study the fluctuations of amino acid positions $\langle \Delta R_i^2(t) \rangle$ around the average value. We follow the procedure of Kabsch and Sanders⁴⁰ and project any evolved conformation onto a reference conformation so that the results are not affected by translation of the center of mass and by rotation of the whole molecule. $\langle \Delta R_i^2 \rangle$ is defined then as $\langle \vec{r}_i^2 \rangle - \langle \vec{r}_i \rangle^2$. The top panel of Figure 6 shows the modulations of $\langle \Delta R_i^2 \rangle$ along the sequence. The largest fluctuations take place at the termini and at $i=12$ where the helix joins the other arm of the hairpin. Smaller, but still substantial, fluctuations occur at $i= 8$ and 15. The data points corresponding to the HI and BD cases nearly overlap indicating the lack of relevance of the HI in the equilibrium fluctuations.

A similar statement applies to the two-point (equal time) characteristics of the motion as illustrated in Figure 7 for pairs of residues i and j that make a native contact. There are 27 such contacts in 112y (counted by the index l) and 13 of them are indicated by the lines in Figure 5. The allocation of the index l to its corresponding pair of i and j is also written underneath the data point in the top panel of Figure 7.

The simplest characteristic is $f_l = (\langle r_{ij}^2 \rangle - \langle r_{ij} \rangle^2)^{1/2}$. This quantity does not depend on any rigid body motion of the protein and it rapidly acquires lack of dependence on the duration of the measurement. The top panel of Figure 7 shows that it is insensitive to the inclusion of the HI. The modulations in the strenghts of f_l span a factor of two. Large values indicate high amplitude oscillations (like in contact 22 between amino acids 7 and 11) and small values point to a relative rigidity (like in contact 27 between 11 and 14). A removal of the "keystone" contact 18 (between residues 6 and 17) is found to reduce f_{22} and f_{15} but to enhance f_5 and f_9 . For an isolated α -helix the f_l s are usually small and uniform except for enhancements at the termini. The β -hairpin has largest fluctuations at contacts that link the termini ($f_l \sim 1.5 \text{ \AA}$).

Another popular characteristic is the so called dynamical cross-correlation map (see e.g. refs.^{24,41,42}) defined as

$$C_l = C_{ij} = \langle \Delta \mathbf{r}_i \cdot \Delta \mathbf{r}_j \rangle / [\langle \Delta \mathbf{r}_i^2 \rangle \langle \Delta \mathbf{r}_j^2 \rangle]^{1/2} . \quad (5)$$

Unlike f_l , C_l involves features which are primarily orientational and does not depend much on the distance between i and j . C_l can be either positive or negative, depending on

the nature of the relative displacement. Its determination requires making the rigid-body transformation that brings the conformation closest to the reference structure. We find that C_l for 112y settles in their stationary values within 2000 τ . These stationary values are shown in the bottom panel of Figure 7. The values of C_l are modulated but the sensitivity to the presence of HI is again seen to be minor.

All of the above single- and double-residue equal time characteristics correlation functions may be also calculated by using the Gaussian network model⁴³ and by performing the normal mode analysis. We find that the nature of the sequence- and pair-dependent modulations coming from this approach is as in Figures 6 and 7 respectively.

2. Time-dependent characteristics

We now take various conformations along each trajectory and investigate what happens to them a time t later. The motion of the center of mass of the protein is subtracted and we could get reasonable statistics for time intervals not exceeding 5000 τ . We define the correlation function

$$S_i(t) = \langle \vec{r}_i(0) \cdot \vec{r}_i(t) \rangle / \langle \vec{r}_i(0) \cdot \vec{r}_i(0) \rangle \quad (6)$$

and $S(t) = \langle S_i \rangle_{av}$, where $\langle \dots \rangle$ denotes an average over the trajectories and $\langle \dots \rangle_{av}$ an average over the residues. The definition implies that for $t=0$, $S_i=1$. The initial decay of $S(t)$ with t is shown in Figure 8. It is seen that the decay, or a 'decoherence', from the initial state is faster, when the HI are included. Due to limitations in statistics at longer delay times, we cannot pinpoint the precise functional law for the time dependence of $S(t)$. However, the important observations is that the time dependence of time correlations is affected by the presence of the HI.

It should be noted here that there exists a puzzle regarding the origin of long-time tails in the correlation functions in proteins. Namely, the experiments by Xie and coworkers⁴⁴ seem to show that fluctuations in proteins decay very slowly in time, following a power law. A number of theoretical attempts to explain this time-dependence have been made^{45,46,47,48} but most of them predict the decay on a much shorter time-scales than those measured in experiments, or perhaps they do not take into account the presence of cross links in the protein.

A related time-dependent characteristic is provided by

$$\Delta_i(t) = \langle [\vec{r}_i(t) - \vec{r}_i(0)]^2 \rangle / \langle\langle [\vec{r}_i(t) - \vec{r}_i(0)]^2 \rangle\rangle_{av} \quad (7)$$

in which the numerator would be related to the single-residue diffusion coefficient, $D_i(t)$, if divided by $6t$. However, this $D_i(t)$ decays to zero, instead of homing in on a constant, since the motion of the center of mass is excluded in the trajectory. By dividing the numerator by the denominator in the expression for $\Delta_i(t)$, one effectively removes most of the time dependence, whether it is provided by BD or by HI. The interesting observation is, as demonstrated in the bottom panel of Figure 6, that $\Delta_i(t)$ shows no difference between BD and HI and, practically, has no time dependence. Its sequential behavior is qualitatively similar to that of $\langle \Delta R_i^2 \rangle$ (the top panel of Figure 6).

In summary, the HI affect the time scale of folding significantly by making the collapse faster through the cooperative action of the drag forces. This phenomenon can be equivalently described by invoking a system with no HI but with a reduced effective viscosity by about a factor of two. Thus in the context of protein folding, or phenomena similar to the flap closing in HIV-1 protease, the presence of HI just shifts the effective value of the damping constant γ . Observing phenomena that can be clearly attributed to the HI may then be difficult experimentally unless one investigates a broad range of temperatures. In an equilibrium evolution, the HI affect time correlation functions without influencing equal time correlations such as the rms fluctuations in the contact length.

This paper has benefited from many fruitful discussions with P. Szymczak who also provided us with his numerical code. We also appreciate discussions with A. Giansanti and M. Wojciechowski. This work has been supported by the grant N N202 0852 33 from the Ministry of Science and Higher Education in Poland.

¹ J. G. Kirkwood and J. Riseman, *J. Chem. Phys.* **16**, 565-573 (1948).

² B. H. Zimm, *J. Chem. Phys.* **24**, 269-278 (1956).

³ P. Mazur and W. van Saarloos, *Physica A*. **115**, 21-57 (1982).

⁴ L. Durlofsky, J. F. Brady, and G. Bossis, *J. Fluid Mech.* **180**, 21-49 (1987).

⁵ B. U. Felderhof, *Physica A*. **151**, 1-16 (1988).

⁶ A. J. C. Ladd, *J. Chem. Phys.* **88**, 5051-5063 (1988).

- ⁷ B. Cichocki, B. U. Felderhof, K. Hinsen, E. Wajnryb, and J. Blawdziewicz, *J. Chem. Phys.* **100**, 3780-3790 (1994).
- ⁸ J. K. G. Dhont, *An Introduction to Dynamics of Colloids*. Elsevier, Amsterdam, (1996).
- ⁹ P. Szymczak and M. Cieplak, *J. Phys.: Condens. Matter.* **19**, 258224 (2007).
- ¹⁰ P. Szymczak and M. Cieplak, *J. Chem. Phys.* **125**, 164903 (2006).
- ¹¹ P. Szymczak and M. Cieplak, *J. Chem. Phys.* **127**, 155106 (2007).
- ¹² M. Cieplak, T. X. Hoang and M. O. Robbins, *Proteins: Struct. Funct. Bio.* **49**, 114-124 (2002).
- ¹³ M. Cieplak, T. X. Hoang and M. O. Robbins, *Proteins: Struct. Funct. Bio.* **56**, 285-297 (2004).
- ¹⁴ J. I. Sułkowska and M. Cieplak, *J. Phys.: Cond. Mat.* **19**, 283201 (2007)
- ¹⁵ J. I. Sułkowska and M. Cieplak, *Bioph. J.* **94**, 6-13 (2008).
- ¹⁶ J. Rotne and S. Prager, *J. Chem. Phys.* **50**, 4831-4837 (1969).
- ¹⁷ H Yamakawa, *J. Chem. Phys.* **53**, 436-443 (1970).
- ¹⁸ N. Kikuchi, J. F. Ryder, C. M. Pooley, and J. M. Yeomans, *Phys. Rev. E* **71**, 061804 (2005).
- ¹⁹ J. F. Ryder, *Mesoscopic simulations of complex fluids*, Ph.D. thesis, the University of Oxford (2005).
- ²⁰ A. Baumketner and Y. Hiwatari, *J. Phys. Soc. Jap.* **71**, 3069-3079 (2002).
- ²¹ J. D. Honeycutt and D. Thirumalai, *Biopolymers* **32**, 695-709 (1992).
- ²² A. Malevantes and R. Kapral, *J. Chem. Phys.* **110**, 8605-8613 (1999).
- ²³ M. Cieplak and T. X. Hoang, *Biophys. J.* **84**, 475-488 (2003)
- ²⁴ W. E. Harte Jr., S. Swaminathan, and D. L. Beveridge, *Proteins: Struct. Funct. Gen.* **13**, 175-194 (1992).
- ²⁵ V. Tozzini, J. Trylska, C. Chang, and J. A. McCammon, *J. Struct. Biol.* **157**, 606-615 (2007).
- ²⁶ J. Trylska, V. Tozzini, C. Chang, and J. A. McCammon, *Bioph. J.* **92**:4179-4187 (2007).
- ²⁷ E. Dickinson, *Chem. Soc. Rev.* **14**, 421-455 (1985).
- ²⁸ H. Abe and N. Go, *Biopolymers* **20**, 1013-1031 (1981). S. Takada, *Proc. Natl. Acad. Sci. USA.* **96**, 11698-11700 (1999).
- ²⁹ T. Veitshans, D. Klimov, and D. Thirumalai, *Folding Des.* **2**, 1-22 (1997).
- ³⁰ H. Nymeyer, A. E. Garcia, and J. N. Onuchic, *Proc. Natl. Acad. Sci. (USA)* **95**, 5921-5928 (1998).
- ³¹ C. Clementi, H. Nymeyer, and J. N. Onuchic, *J. Mol. Biol.* **298**, 937-953 (2000).
- ³² T. X. Hoang and M. Cieplak, *J. Chem. Phys.* **112**, 6851-6862 (2000).

- ³³ J. I. Sułkowska and M. Cieplak, *Biophys. J.* **95**, 3174-3191 (2008).
- ³⁴ D. L. Ermak and J. A. McCammon, *J. Chem. Phys.*, **69**, 1352-1360 (1978).
- ³⁵ J. Garcia de la Torre and V. A. Bloomfield, *Quarter. Rev. Biophys.* **14**, 81-139 (1981).
- ³⁶ J. Antosiewicz and D. Porschke, *J. Phys. Chem.* **93**, 5301-5305 (1989).
- ³⁷ A. A. Zamyatin, *Prog. Biophys. Mol. Biol.* **24**, 107-123 (1972).
- ³⁸ J. Antosiewicz – private communication.
- ³⁹ P. Szymczak and M. Cieplak, NIC Workshop 2007 From Computational Biophysics to Systems Biology 2007, ed. U. H. E. Hansmann, J. Meinke, S. Mohanty, and O. Zimmerman, NIC Series Volume 36, 1-7 (2007).
- ⁴⁰ W. Kabsch and C. Sander, *Biopolymers.* **22**, 2577-2637 (1983).
- ⁴¹ G. Chillemi, P. Fiorani, P. Benedetti, and A. Desideri, *Nucl. Acid. Res.* **31**, 1525-1535 (2003).
- ⁴² F. Pizzitutti, A. Giansanti, P. Ballario, P. Ornaghi, P. Torreri, G. Ciccotti, and P. Filetici, *J. Mol. Recognit.* **19**, 1-9 (2006).
- ⁴³ I. Bahar, A. R. Atilgan, and B. Erman, *Folding and Design.* **2**, 173-181 (1997).
- ⁴⁴ W. Min, G. B. Luo, B. J. Cherayil, S. C. Kou, and X. S. Xie, *Phys. Rev. Lett.* **94**, 198302 (2005).
- ⁴⁵ R. Granek and J. Klafter, *Phys. Rev. Lett.* **95**, 098106 (2005).
- ⁴⁶ J. Tang and R. A. Marcus, *Phys. Rev. E.* **73**, 022102 (2006).
- ⁴⁷ J. Tang and S. H. Lin, *Phys. Rev. E.* **73**, 061108 (2006).
- ⁴⁸ J. H. Xing and K. S. Kim, *Phys. Rev. E.* **74**, 061911 (2006).

FIGURE CAPTIONS

Fig. 1. The median folding times as a function of temperature for the three proteins. The dotted lines and open data points correspond to the BD model whereas the solid lines and data points to the model with the HI. The hydrodynamic radius is 1.5 Å. The f -factors on the right give the ratios of the optimal folding times without the HI to those with the HI.

Fig. 2. Top panel: The distribution of single trajectory folding times at $k_B T/\epsilon=0.3$ for the model crambin. Bottom panel: Examples of time evolution of the radius of gyration. The down-pointing arrows indicate entries into the phase of compact collapsed conformations. The up-pointing arrows show arrivals at the native conformation.

Fig. 3. The scenario diagram for folding of the model 1crn. The hexagons correspond to the time to establish the contacts between C and I for the first time. The circles correspond to the contacts between two β -strands. The full circles - to the contacts within helices and between helices. The asterisks correspond to all other contacts. The upper symbols involve the HI and the lower do not.

Fig. 4 The flap dynamics in 1a30 as discussed in the main text. The conformation on the right is native and on the left is stretched. The dotted line corresponds to the BD case and is based on 50 trajectories. The solid line corresponds to the HI case and is based on 20 trajectories, all starting from the same stretched state.

Fig. 5. The native state of 1l2y. The larger numerical symbols enumerate the amino acids from the N terminal. The smaller symbols enumerate native contacts (the C-terminal generates no native contacts). The contacts are also indicated by lines. The solid lines correspond to contacts with strong distance fluctuations, as shown in Figure 6, whereas the dashed lines to those with weak fluctuations.

Fig. 6. Top panel: Variance in single-residue position fluctuations as enumerated sequentially. The solid (open) symbols are for the model with (without) the HI and $k_B T/\epsilon=0.3$. Bottom panel: normalized time-dependent variance $\Delta_i(t)$ for $t = 1000\tau$. The symbols corresponding to HI and BD in this and following two figures are displaced laterally around the proper position to enhance their individual visibility.

Fig. 7. Fluctuations in the native contacts around the native state at $k_B T/\epsilon=0.3$. Top panel: the distance rms fluctuations. The numbers indicate pairs of amino acids that are connected by the native contact labeled by l . Bottom panel: the orientational rms fluctuations (known also as the dynamical cross-correlations).

Fig. 8. The normalized time correlation $S(t)$ as a function of time.

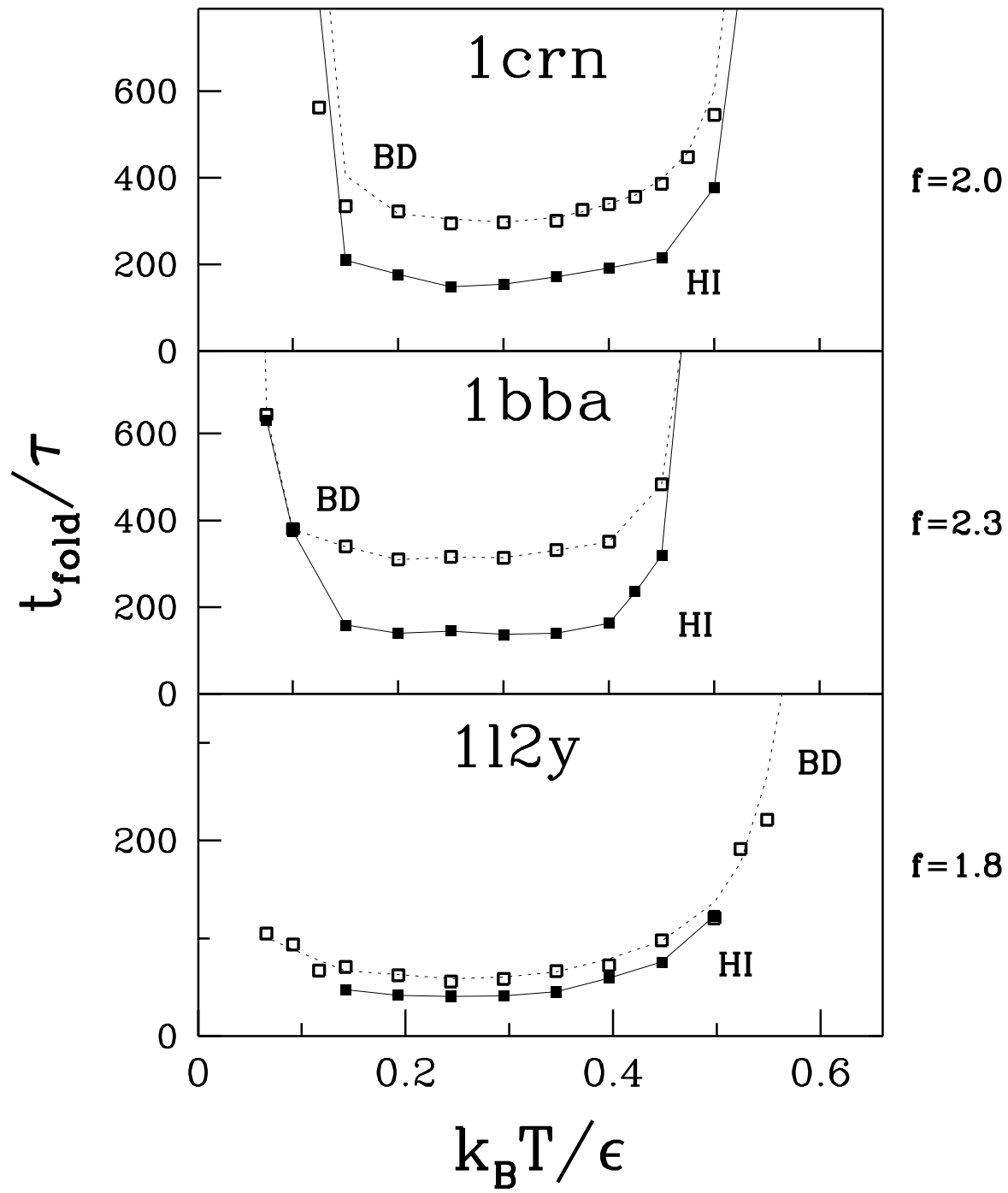


FIG. 1:

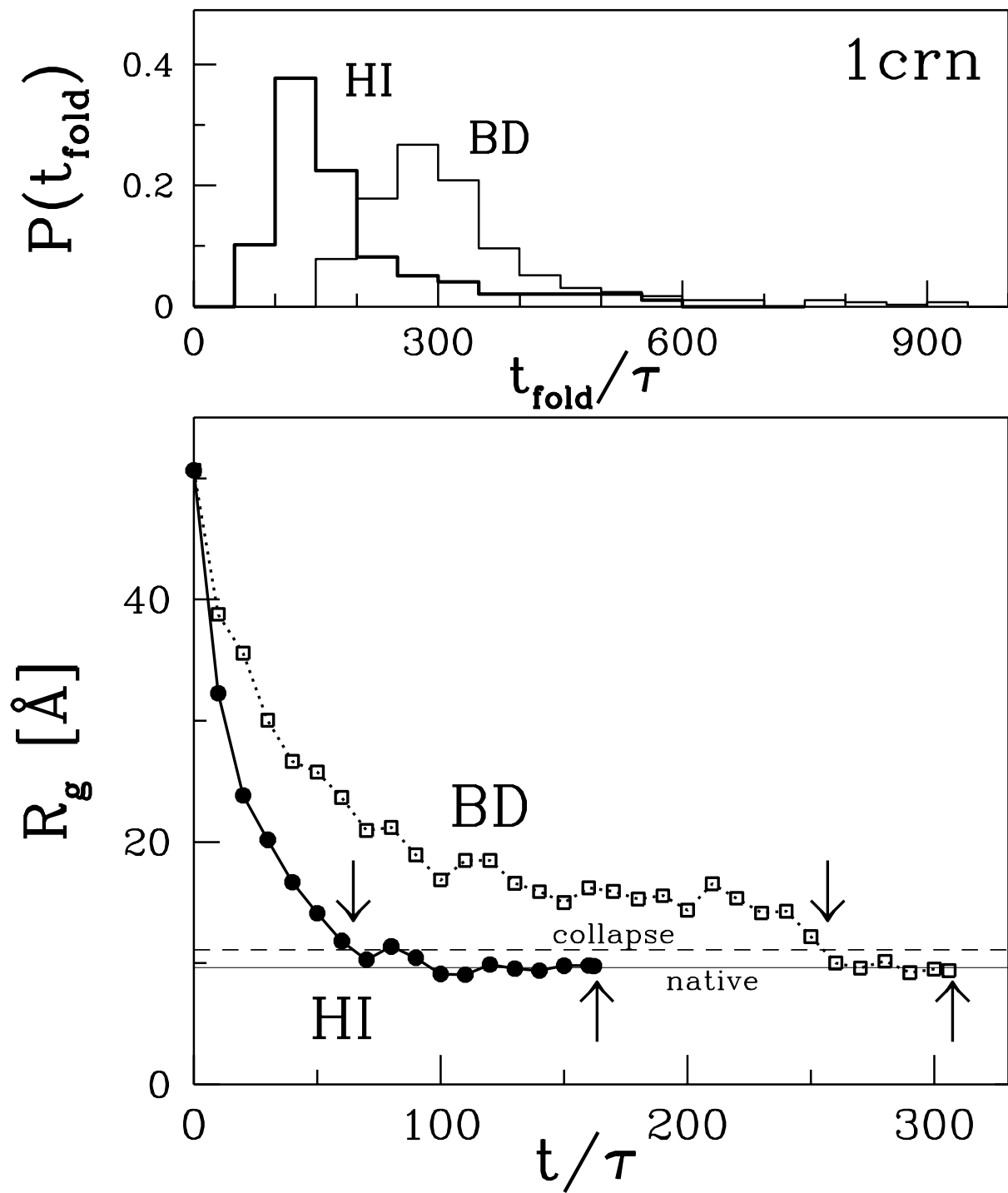


FIG. 2:

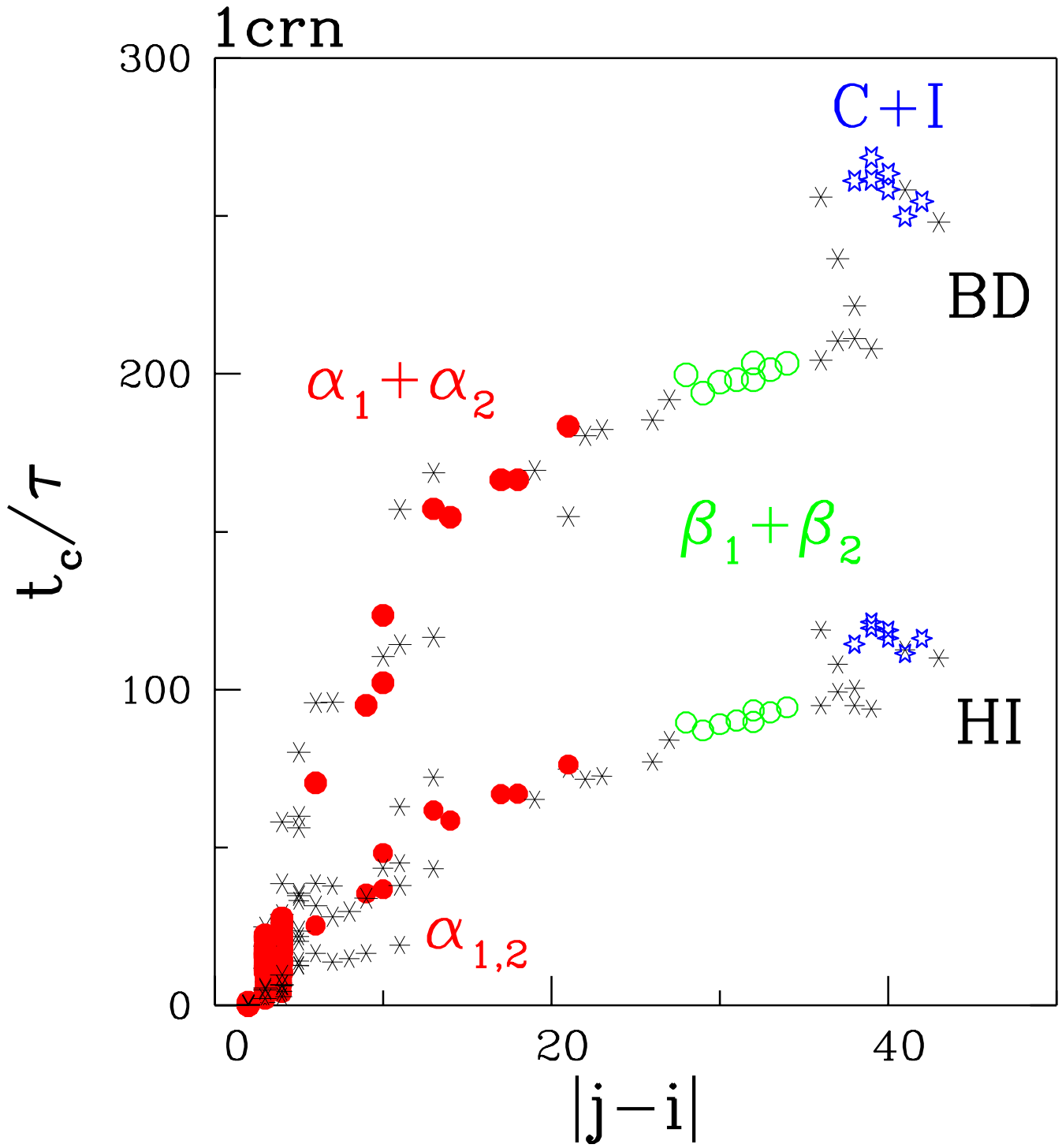


FIG. 3:

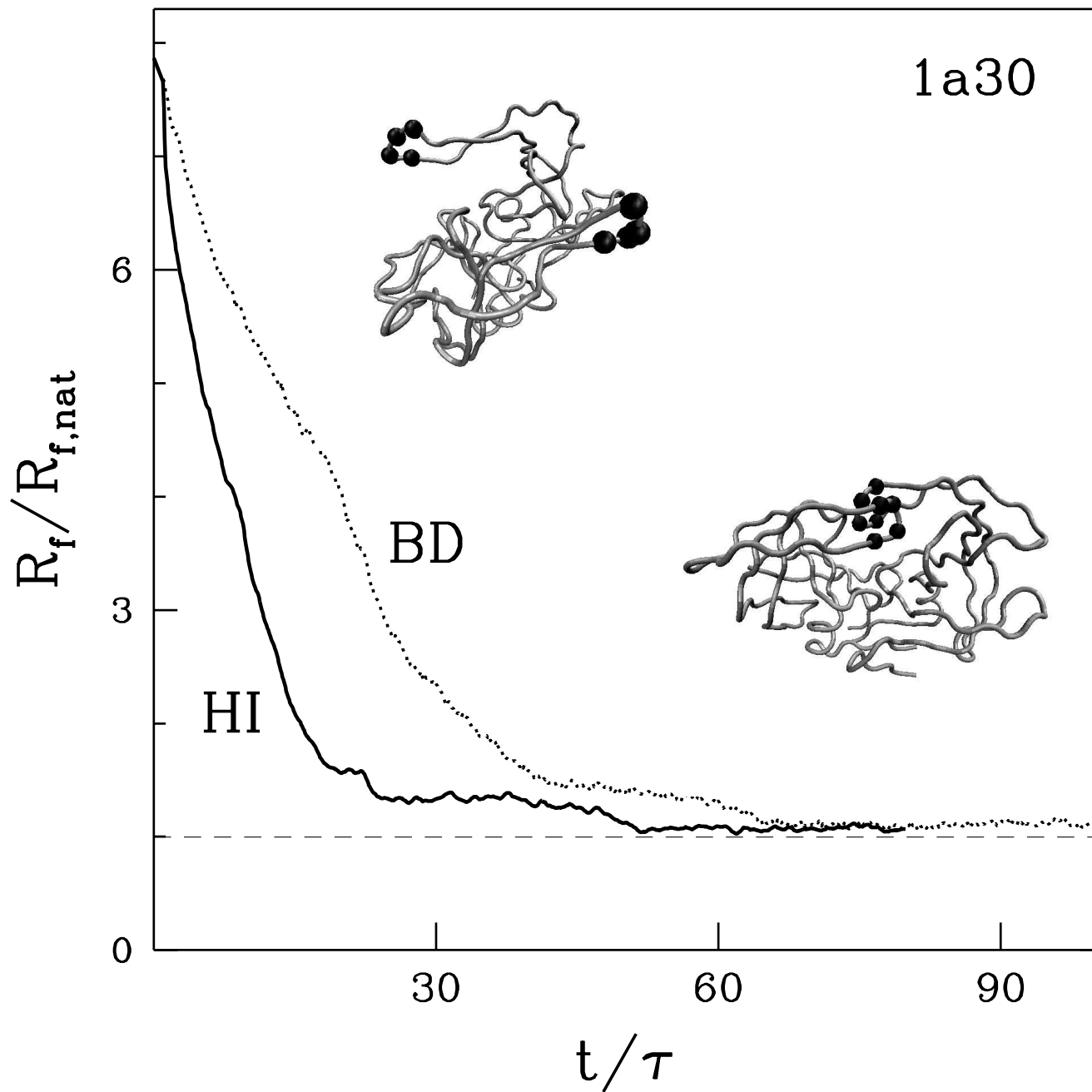


FIG. 4:

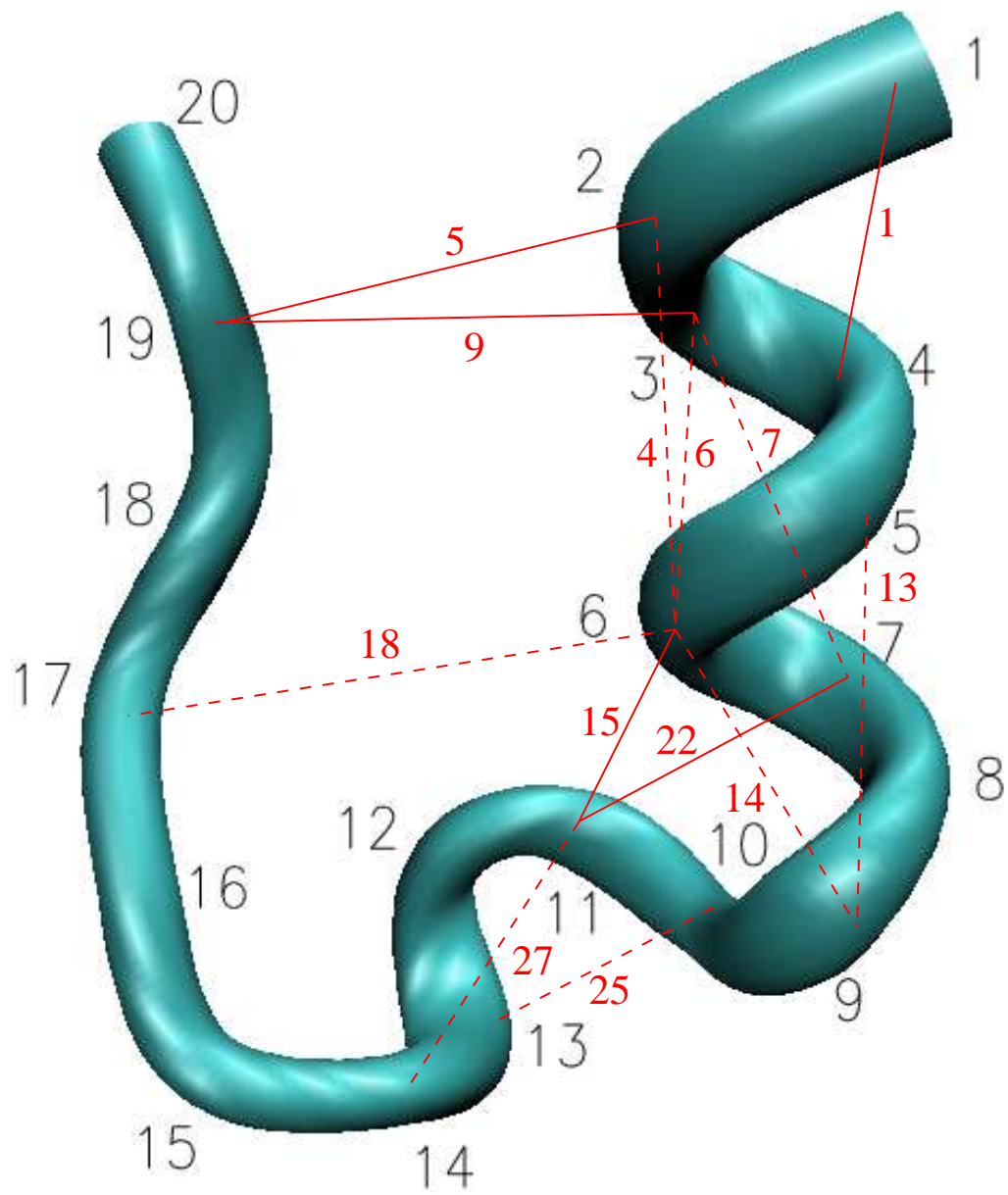


FIG. 5:

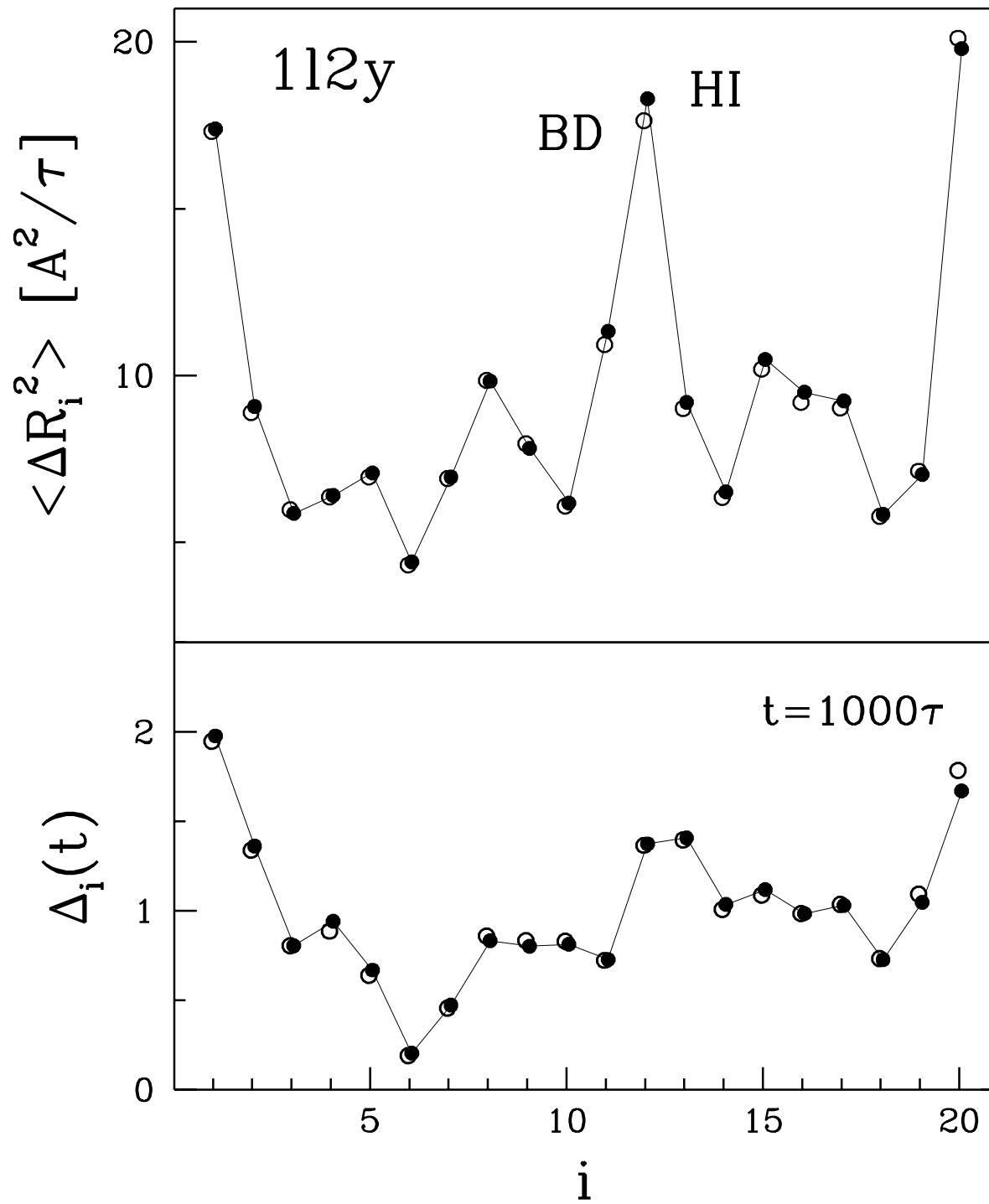


FIG. 6:

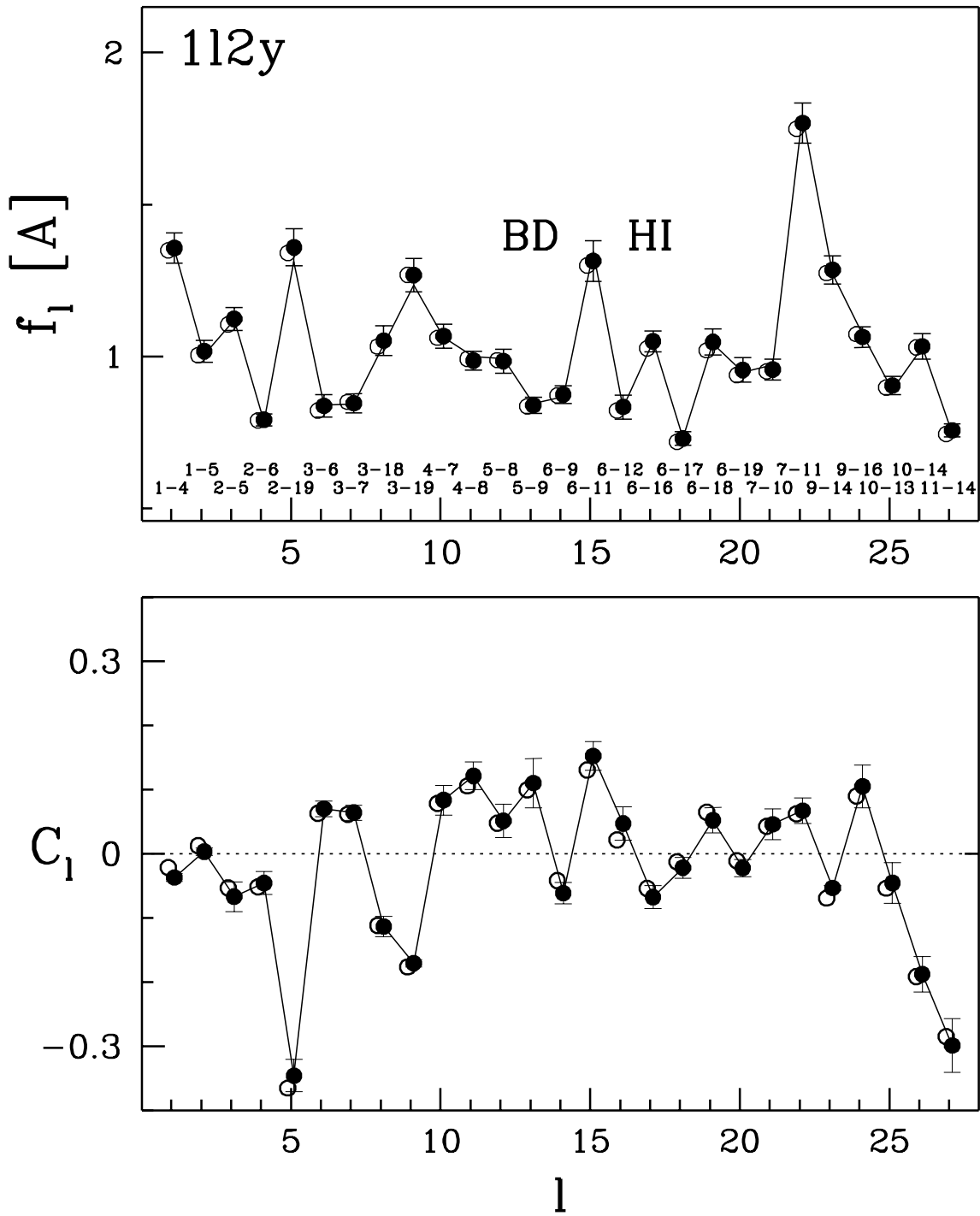


FIG. 7:

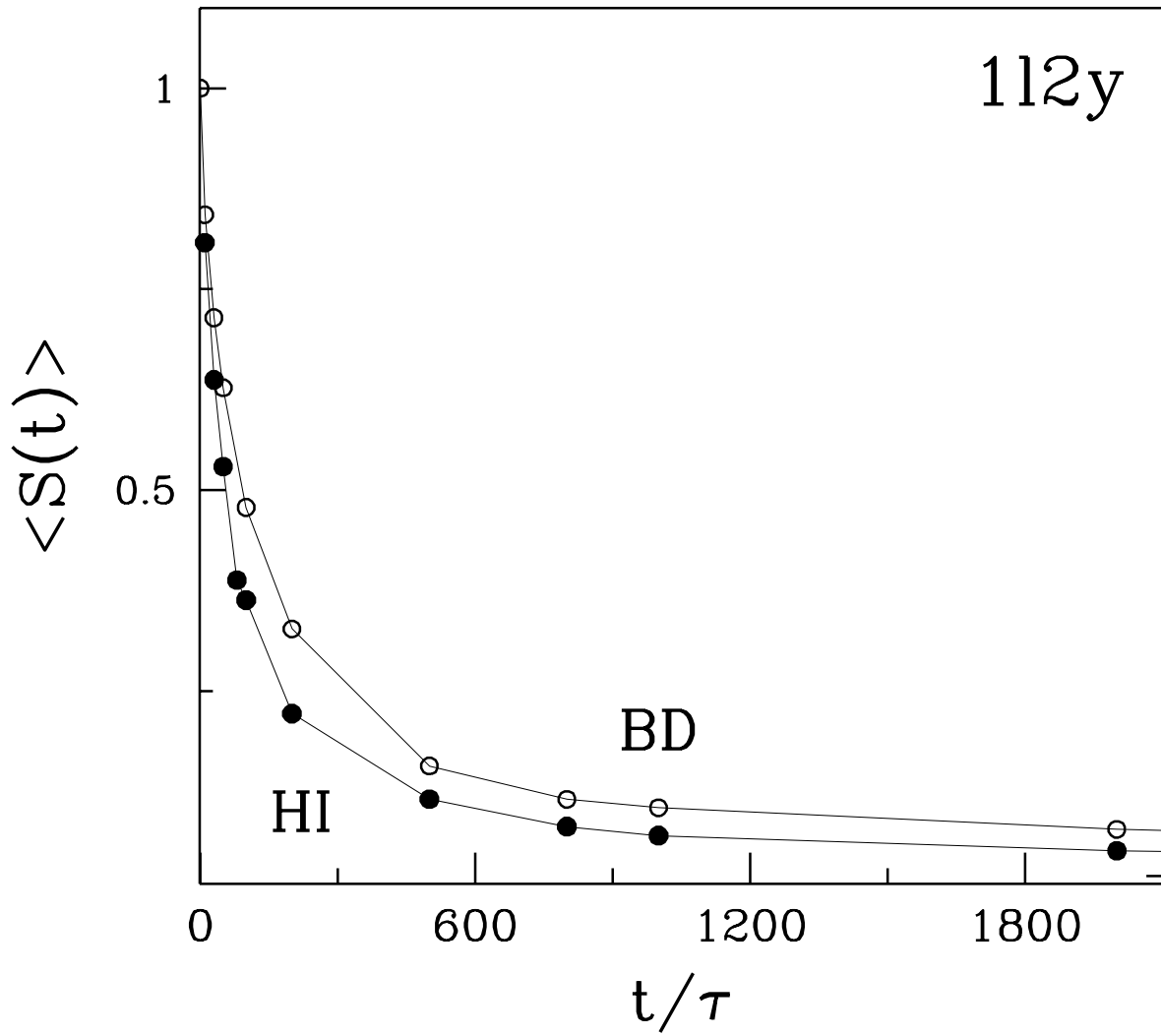


FIG. 8: